Nanodomains of I_α and I_β Cellulose in Algal Microfibrils

Tomoya Imai and Junji Sugiyama*

Wood Research Institute, Kyoto University, Uji, Kyoto 611-0011, Japan

Received April 23, 1998; Revised Manuscript Received July 9, 1998

ABSTRACT: Ultrastructural localization of cellulose I_α and I_β allomorphs in one microfibril from algal sources was investigated using electron microdiffraction. Both cellulose I_α and I_β were characterized as one-chain triclinic and two-chain monoclinic unit cells, respectively, in agreement with previous studies. These two structures coexisted in each microfibril, alternating either longitudinally or laterally. The transition zone between the two phases was found to be the interface between adjacent H-bonded molecular sheets (i.e., 0.39-nm lattice planes).

Introduction

Native cellulose is known to be a composite of two distinct allomorphs, I_α and I_β, whose fractions vary depending on the biological origin.[1,2] Using electron microdiffraction analysis, the corresponding crystallographic units were characterized as one-chain triclinic and two-chain monoclinic unit cells, respectively,[3] with both phases coexisting in a single microfibril. The diagrams from circular regions of the specimen 20−100 nm in diameter were recorded successively along the molecular axis of a microcrystal isolated from cell walls of the green marine alga, *Microdictyon tenuius*.[3] The diffraction patterns often demonstrated the existence of a transition from monoclinic regions to triclinic ones, with mixed patterns found in between. Thus, a microfibril model where the two domains coexist alternatively along the microfibrillar axis was envisaged.

The localization of the two crystalline domains is of importance to the understanding of the mechanism of crystallization as well as the biosynthesis of cellulose microfibrils. However, it is not straightforward to draw a general model for cellulose microfibrils, partly because of the structural diversity depending on origin and partly because of a lack of a direct method for analysis. Atalla et al.[4,5] investigated the structure of nascent bacterial cellulose ribbons incubated in the presence of hemicellulosic materials. Addition of such molecules resulted in the formation of I_β-rich fibrillated subfibrils that were different from I_α-rich ribbons in normal culture conditions. A microfibril model was then proposed where the I_β core subfibrils were packed in the superlattice of the I_α domain to form a ribbon-shaped microfibril.[5] The model seems to explain well the selective crystallization into I_α and I_β of higher plant celluloses in terms of hemicellulosic deposition. However, electron diffraction obtained from *M. ternuius*[3] did not support the existence of such a superlattice. More recently, Yamamoto et al.[6] proposed that I_α crystallized under the stress induced by the natural twisting behavior of bacterial cellulose ribbons. In this model, the central part of the ribbon, the twisting axis of the corresponding ribbon, is considered to be rich in I_β and the I_α fraction is considered to increase in proportion to the distance from the center. If this is the case, I_α and I_β domains should be localized laterally rather than longitudinally.

* To whom correspondence should be addressed. Fax: 81-774-38-3635. E-mail: junjis@kuwri.kyoto-u.ac.jp.

These results on the ultrastructure of bacterial cellulose microfibrils stimulated us to further investigate the microfibrils of a series of green marine algae. We selected *Cladophora*, *Valonia*, and *Boergesenia* because the cellulose microfibrils of these species have been widely used for structural studies as standard highly crystalline materials. The microfibrils were hydrolyzed to form microcrystals, which were probed by precise microdiffraction to clarify how triclinic (I_α) and monoclinic (I_β) domains intermingled within a given microcrystal.

Experimental Section

Materials. Three marine green algae, namely, *Cladophora* sp., *Valonia ventricosa*, and *Boergesenia forbesii*, were used as typical I_α-rich cellulose samples. *B. forbesii* was cultivated in the artificial marine water, Marine Art (Senju Seiyaku Co., Japan) with ES medium,[7] while the other two were respectively harvested from the sea bed in Chikura, Chiba, Japan (*Cladophora* sp.) and in the Lower Keys, FL (*V. ventricosa*). In comparison, microfibrillated tunicate cellulose from the tunic of *Halocynthia roretzi* (supplied by Daicel Chem. Co., Tokyo, Japan) was used because it consists mostly of I_β phase.[8,9]

Sample Preparation. Purification and Preparation of Microcrystals. The sample was purified either by boiling in 0.05 N NaOH for 8 h followed by immersion in 0.05 N HCl for 12 h at room temperature or by immersion in 1% KOH for 12 h at room temperature before a treatment in 0.3% $NaClO_2$ buffered at pH 4.9 with acetate buffer for 3 h at 70 °C. The purification process was carefully monitored by FT-IR (described later) from the attenuation of 1600-cm^{-1} absorbance of noncellulosic contaminants. The purified sample was then hydrolyzed either by boiling in 2.5 N HCl for 12 h, or by gentle stirring in 40% (w/v) H_2SO_4 for 3 days at 70 °C, followed by dialysis after several washes in distilled water by centrifugation. Neither a structural nor a spectroscopic difference was detected between these preparations.

For the preparation of I_β-dominant microcrystals, a portion of the purified algal microcrystals was subjected to a hydrothermal treatment.[10] For this, the specimen was autoclaved in a high-pressure bomb at 260 °C for 30 min in the presence of aqueous 0.1 N NaOH.

Infrared Spectroscopy. The suspension of microcystals was deposited on a glass slide and allowed to dry. A thin membrane was floated off onto water and mounted over the sample holder perforated by a 5 mm hole. The Jasco FT-IR 7000 spectrometer was used in the absorbance mode with 4-cm^{-1} resolution and 16 times integration in the range of 4600−400 cm^{-1}.

Transmission Electron Microscopy. A drop of the microcrystal suspension was deposited on carbon-coated Cu grids and allowed to dry. The sample was observed with a

S0024-9297(98)00664-0 CCC: $15.00
Published on Web 08/19/1998

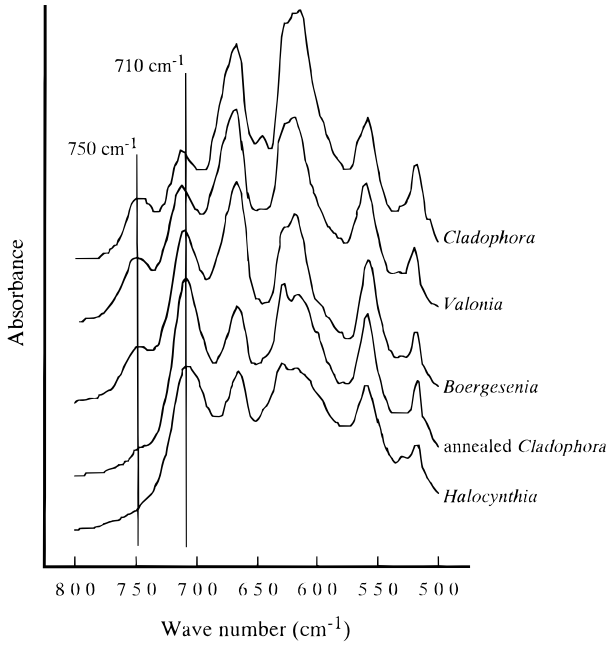

Figure 1. FT-IR spectra of the specimens in the region of 500−800 cm^{-1}. The absorbances at 750 and 710 cm^{-1} are characteristic of I_α and I_β, respectively.

JEOL JEM-2000EX II microscope operated at an accelerating voltage of 100 kV. The image was taken under diffraction contrast in the bright-field mode without prior contrast enhancement, using a low-dose exposure. For diffraction analysis, the microdiffraction technique was primarily used.[3] To obtain an approximately 100-nm-diameter electron probe, a 20-μm aperture was inserted in the condenser lens field and the first condenser was fully excited. The sample was observed under extremely low dose illumination with the help of a GATAN image intensifier. When an area of interest was found, the probe was focused to its smallest size (approximately 100 nm diameter) and at the same time the dose was reduced to the minimum required for identification on the TV monitor. As soon as the sample was localized, the beam was blanked to prevent any unnecessary irradiation prior to image recording. Conventional selected-area electron diffraction diagrams were also taken from the area of about 2-μm diameter in the specimen. All the images and diffractograms were recorded on Mitsubishi electron microscope films (MEM).

Results and Discussion

FT-IR Measurement. All the FT-IR spectra obtained from purified samples were well-resolved and almost free of noncellulosic contaminants. Enlarged spectra in the region from 800 to 500 cm^{-1} are shown in Figure 1. Estimation of the I_α fraction was carried out using the integrated intensities of the two absorbance peaks at 750 and 710 cm^{-1} that are respectively characteristic of I_α and I_β allomorphs.[11] Assuming that the absorptions at the above two peaks are proportional to the mass of I_α and I_β allomorphs, the I_α fraction was written as

$$f_\alpha = A_{750}/(A_{750} + kA_{710})$$

where k is the ratio of adsorption coefficients (ϵ) between two peaks ($k = \epsilon_{750}/\epsilon_{710}$). In this study, k was estimated to be 0.16 by assuming an f_α value of 0.64 for *V. ventricosa*.[12] As summarized in Table 1, *Cladophora* sp. cellulose was found to be the richest in I_α, followed by *V. ventricosa* and *B. forbesii* cellulose. Annealed *Cladophora* sp. was estimated to be 0.24, which is larger than the previously reported values of annealed *V. macrophysa* by ^{13}C NMR.[12]

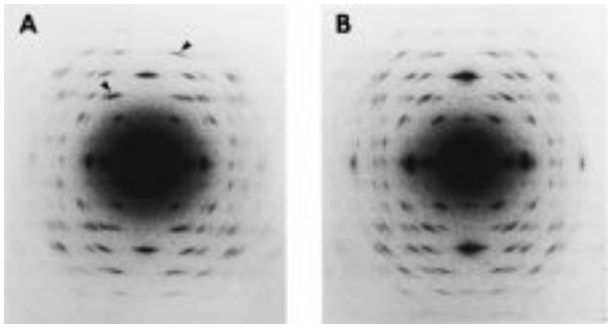

Figure 2. Selected area electron diffraction fiber diagrams obtained from original (A) and annealed (B) *Cladophora* sp. Note that the arrowheads indicate typical triclinic asymmetrical reflections on the third and fifth layer lines.

Table 1. I_α Fractions in Specimens of Various Origins

sample	I_α fraction	±SE[a]
Cladophora sp.	0.76	±0.01
V. ventricoa	0.64[12]	±0.01
B. forbesii	0.55	±0.01
annealed *Cladophora* sp.	0.24	±0.03
Halocynthia sp.	0[8]−0.10[9]	

[a] Standard error ($n > 8$).

Taking the abundance of I_α allomorph and the large crystal size (20−30 nm) into account, *Cladophora* sp. cellulose was extensively investigated with further electron microscopy, while the others were used complementarily.

Electron Diffraction. Figure 2 shows typical selected-area fiber-diffraction diagrams obtained from a delaminated cell wall of both initial and annealed *Cladophora* sp. Apparently the diffraction patterns are easily distinguishable especially by the intensities on the third layer line and meridians as reported for *V. ventricosa*. Initially (Figure 2A), the triclinic character was well-demonstrated due to asymmetrical diffraction spots occurring in the upper-left-hand and upper-right-hand quadrants, as indicated by arrowheads. Upon annealing, the pattern became simpler, as shown in Figure 2B, where the initial triclinic character changed to a monoclinic one. This was accompanied by an increase of the $(002)_m$[13] meridional intensity. Such structural features were identical with those obtained with the previous *V. ventricosa*[14] and *M. tenuius*[3] celluloses.

More than 200 microdiffraction diagrams from initial *Cladophora* sp. microcrystals were analyzed. A typical example is presented in Figure 3 where the diagram on the left exhibits perfect triclinic symmetry while that on the right corresponds to a monoclinic b^*c^* pattern. The analysis of all the diagrams confirmed the general concept that the microfibril possesses two domains, namely, one-chain triclinic and two-chain monoclinic crystals. The unit cell parameters obtained from *Cladophora* sp. cellulose were $a = 0.670$ nm, $b = 0.595$ nm, and $c = 1.036$ nm (chain axis), $\alpha = 118°$, $\beta = 114°$, and $\gamma = 79.7°$ for the one-chain cell (calculated over 25 independent reflections), and $a = 0.798$ nm, $b = 0.809$ nm, and $c = 1.036$ nm, $\gamma = 96.8°$ for the two-chain cell (16 reflections). These parameters were quite similar to the previous data obtained from *M. tenuius* cellulose [$a = 0.674$ nm, $b = 0.593$ nm, and $c = 1.036$ nm (chain axis), $\alpha = 117°$, $\beta = 113°$, and $\gamma = 81°$ for the one-chain

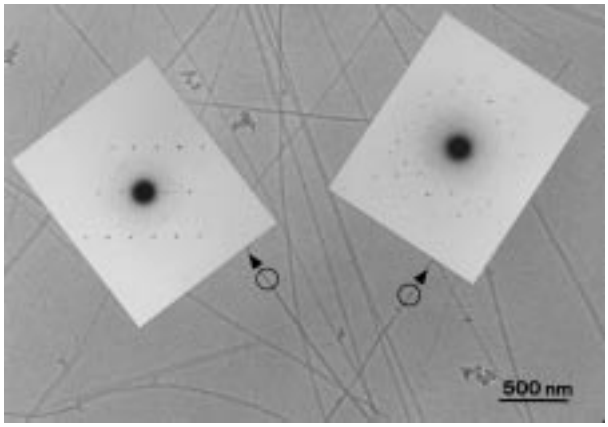

Figure 3. Typical specimen preparation of *Cladophora* sp. cellulose microfibrils together with microdiffraction patterns from the ca. 100-nm-diameter region. The diagram on the left shows one from the triclinic crystals, while that on the right shows one from the monoclinic crystals.

cell (calculated over 27 independent reflections)] but slightly different from $a = 0.801$ nm, $b = 0.817$ nm, and $c = 1.036$ nm, $\gamma = 97.3°$ for the two-chain cell (38 reflections). As in the case of *M. tenuius* , *d* spacing data from an annealed cellulose were incorporated for refinement of the I_β cell parameters; the variation in parameters may reflect structural differences and/or imperfections between initial and annealed I_β cellulose crystals.

Single-phase diagrams, such as the one showing pure triclinicity as on the left-hand side of Figure 3, were less frequently observed than in the case of *M. tenuius* cellulose. In most cases, diagrams contained diffraction spots from two structures: the ratio of the two structures was found to vary, although we could not measure their relative amounts. This observation implies either that in *Cladophora* sp. cellulose, the two phases are more intimately associated with each other than in *M. tenuius* cellulose or that the electron probe diameter in this study (ca. 100 nm) may have been too large.[3] To rule out the latter technical problem, we tested the same sample with an analytical electron microscope (JEOL JEM-2010) equipped with imaging plates (Fuji Film, Tokyo, Japan).[15] Microdiffraction diagrams from circular areas of 20 nm in diameter were successfully recorded on a microfibril (not shown here) and gave results similar to those above. Therefore, we concluded that the two crystalline domains were more intimately associated than those in the case for *M. tenuius*.

Among the diagrams which contain both triclinic and monoclinic spots, the projection parallel to the equatorial 0.39-nm lattice planes and perpendicular to the fiber axis has a unique character. It corresponds to the projection along the $[1\bar{1}0]$ zone axis in the case of the triclinic unit cell and along [010] of the monoclinic unit cell, where the difference in the translation of adjacent cellulose chains between triclinic and monoclinic unit cells can be clearly detected (see Figure 6B, for instance). Since the chains in equatorial 0.39-nm lattice planes are H-bonded to form molecular sheets, the shift of chains can be regarded as the shift of molecular sheets. According to the previous model,[3] this shift between molecular sheets in the triclinic domain is unidirectional ($c/4$, $c/2$, $3c/4$, c, $5c/4$, ...), whereas that in the monoclinic domain is alternating ($c/4$, 0, $c/4$, 0, ...).

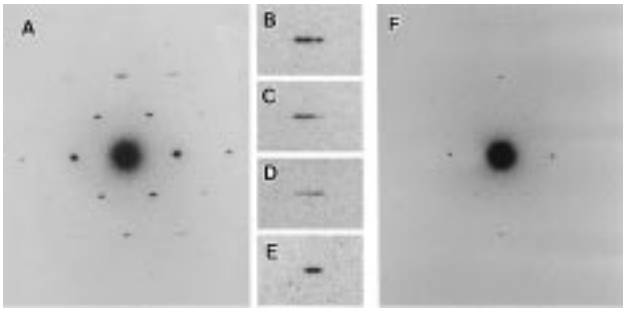

Figure 4. Microdiffraction diagrams obtained from the projection perpendicular to the fiber axis and parallel to the 0.39-nm lattice planes. Zone axes are defined as $[1\bar{1}0]$ for the triclinic diagrams and [010] for the monoclininc diagrams. The fiber axis is vertical. A was obtained from initial *Cladophora* sp., and that in F was obtained from *Halocynthia* sp. B−E show the enlarged meridional reflections from initial *Cladophora* sp., *V. ventricosa*, *V. ventricosa*, and *B. forbesii*, respectively.

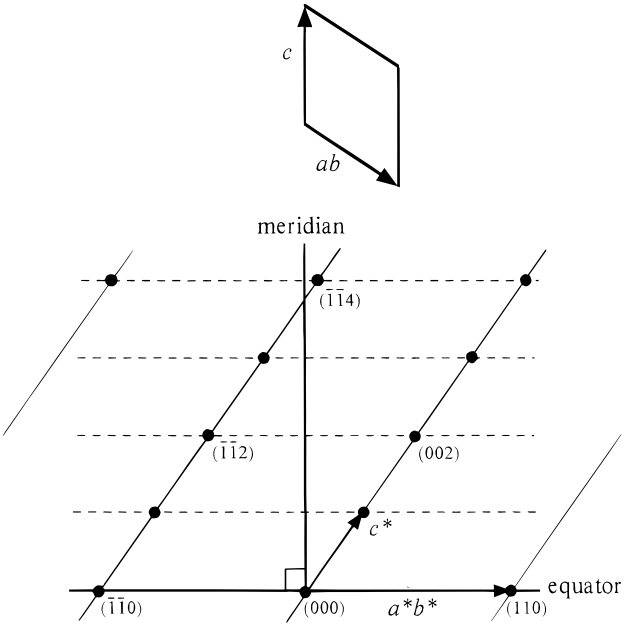

Figure 5. Schematic representation of the real and reciprocal lattice in the same projection as in Figure 4. Note that the triclinic $(\bar{1}\bar{1}4)_t$ is not exactly on the meridian.

Typical electron diffraction diagrams obtained from such a situation are shown in Figure 4. Surprisingly, three meridional reflections (ca. 0.26 nm) were observed in most experiments with *Cladophora* sp. cellulose Figure 4A,B). These are merged into one streaky peak in selected-area diffractions (for example, see Figure 2A). The one in the center was assigned to $(004)_m$ reflection from the monoclinic region, while the other two were assigned to $(\bar{1}\bar{1}4)_t$ from the triclinic region. This phenomenon was not observed in the case of tunicate cellulose, which consists mostly of I_β monoclinic cellulose (Figure 4F) and therefore is specific to I_α-rich cellulose. As shown in the enlarged meridional spots (Figure 4B−E), the number of spots varies from area to area, although there are at least two spots in most cases.

Based on the published model[3] as well as on the unit cell parameters obtained from this study, the triclinic reciprocal net in the corresponding projection that gave the pattern in Figure 4 was schematically represented in Figure 5. The $(\bar{1}\bar{1}4)_t$ spot, slightly to the right of the meridian, clearly indicates that the triclinic *ab* plane

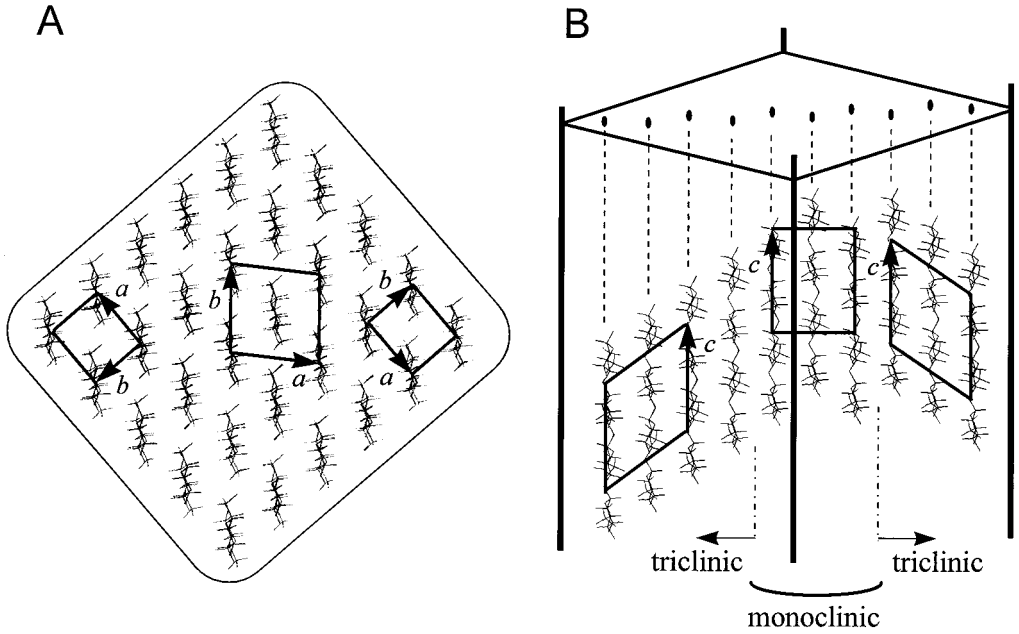

Figure 6. Packing of a 0.39-nm molecular sheet in a microfibril having two triclinic domains separated by a monoclinic domain. A: view along the chain direction. B: view along [1$\bar{1}$0] (triclinic) and [010] (monoclinic) directions.

slopes from top-left to bottom-right. Accordingly, the corresponding plane is from top-right to bottom-left when the $(\bar{1}\bar{1}4)_t$ spot appears on the left side. On the other hand, monoclinic $(004)_m$ appears exactly on the meridional axis. Thus, the nature of the three spots in the meridian is well-explained.

The molecular packing that gives the diffraction diagram in Figure 4A can be schematically drawn as in Figure 6B. In this projection, the structural differences between triclinic and monoclinic units are quite clear in that the asymmetric unit, i.e., cellobiose, in the triclinic system, shows unidirectional shifts of *c*/4 between adjacent molecules, whereas in the monoclinic system, it shows alternatively up and down *c*/4 translations. Assuming that the direction of the triclinic *ab* slope is altered (i.e., downward to upward) in the middle of the microfibril, two triclinic crystals can be drawn, one being obtained from the other by a 180° rotation around the *c* axis, followed by a *c*/2 translation along the *c* axis. Interestingly, one can notice that the chain packing between these two triclinic domains has, in fact, monoclinic characteristics. Furthermore, we did not find any defect as seen in the projection parallel to the chain direction (Figure 6A), which is consistent with the previously reported cross-sectional images on algal cellulose microfibrils.[16,17]

Figure 7 is a schematic representation of the relationship between the shift of chains and the corresponding diffraction patterns. Diagrams A−C of Figure 7 show triclinic/monoclinic composites, while Figure 7D is a fully monoclinic crystal. In *Cladophora* sp. and *V. ventricosa* cellulose microfibrils, situation A of Figure 7 was the most frequently observed, followed by Figure 7B. When the translational shift is frequently altered as in Figure 7B, a microfibril consists of multiple domains of both triclinic and monoclinic crystals. In such a case, the streaking of the meridional diffraction spot occurs perpendicularly to the translational defects, the interfaces between triclinic and monoclinic domains. This phenomenon was sometimes observed in the case of *Cladophora* sp. and *V. ventricosa*. As for *B. forbesii* cellulose, the diagram of two spots, shown in Figure 7C,

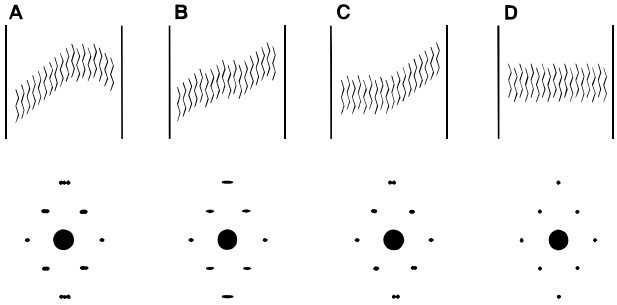

Figure 7. Probable molecular sheet packing explaining the difference in the diffraction diagrams in Figure 5. Each line indicates cellotetraose. A: two triclinic domains with a monoclinic domain in between. B: multiple domains of triclinic and monoclininc domains. C: triclinic and monoclinic domains. D: a perfect monoclinic domain.

was most frequent. Though the above explanations do not include all the situations and may be oversimplified, it is helpful to understand how the directionality and frequency of the translational shifts result in the formation of nanodomain structures consisting of I_α and I_β.

To summarize, the two allomorphs in algal celluloses consist of crystalline domains along the molecular direction. These domains can coexist alternatively both along the microfibril length and across laterally. When they coexist laterally, the interface between the two domains would be the H-bonded molecular sheets of cellulose. The detailed manner in which these two domains intermingle seemed also to vary depending on the algal cellulose origins.

Ultrastructural aspects of acetylation of *V. ventricosa* and *Halocynthia* sp. celluloses were investigated by electron microscopy, and a considerable reduction in the diameter of the crystalline domain was observed[18] due to a continuous stripping of the surface chains as they became acetylated. Interestingly, during the initial stage of acetylation, the cross-sectional shape of *V. ventricosa* crystals became smaller polygonal as if some part of its lateral face had been specifically and sharply wedged off, while that of *Halocynthia* sp. crystals was

evenly rounded. This process was further investigated by ^{13}C NMR and FT-IR[19] respectively by deconvoluting the C1 resonance and the absorbance at 3240 and 3270 cm^{-1} into the fractional amount of I_α, and both measurements showed that the I_α crystals were more susceptible to acetylation. These results allow us to envisage that in *V. ventricosa*, there are multiple intermingled domains separated by crystallographic boundaries as assumed in our model. Furthermore, the area closer to the surface would be primarily occupied by the I_α allomorph as is also suggested by high-resolution atomic force microscopy imaging on *V. ventricosa* microcrystals.[20]

As the enzymatic degradation of cellulose allomorphs is another important method to deduce structural information, the crystalline and morphological structures of *Cladophora* sp. and *Halocynthia* sp. celluloses during hydrolysis by *Trichoderma* sp. cellulase were investigated.[21] Again, at the initial stage of hydrolysis, the I_α crystalline component was more rapidly and selectively degraded than I_β crystals. The ultrastructural appearance of residual cellulose crystallites after hydrolysis was also found different: *Cladophora* sp. microcrystals became shortened and fibrillated, whereas *Halocynthia* sp. microcrystals were primarily fibrillated. The results favor that, in *Cladophora* sp. cellulose I_α and I_β domains would localize alternatively along the microfibril axis.

The model proposed here, where two structures coexist in each microfibril, alternating either longitudinally or laterally, having interfaces between adjacent H-bonded molecular sheets, is still speculative. However, we believe it is most suitable to explain all the details in diffraction data of algal cellulose investigated here as well as the above-mentioned acetylation and enzymatic degradation experiments.

In vitro[22] and abiotic[23] synthesis of cellulose has generated extremely thin microfibrils (about 1.1−1.3 nm), suggesting that cellulose sheet formation was the first stage of microfibril formation. Recent molecular dynamics simulations[24] reported that the molecular sheet bonded by van der Waals forces was the first to form. The second step of crystallization was the piling up of the sheets to form a squarish or rectangular cross section. If this is the case, one would have difficulty building up the translation that we proposed in our model. Study is in progress to improve our microfibril model in order to explain biosynthesis, crystallization, surface structure, and chemical and enzymatic accessibilities of algal cellulose.

Acknowledgment. We are indebted to Drs. H. Chanzy and J.-L. Putaux for their critical reading of the manuscript. We also thank Dr. Oikawa, Akishima, JEOL, Japan, for the experiment with JEM-2010 equipped with imaging plates. The study was supported by the joint research program between JSPS and CNRS and in part by the Grant-in-Aid for Scientific Research (No. 07456156). T.I. was a Research Fellow of the Japan Society for the Promotion of Science.

References and Notes

(1) Atalla, R. H.; Vanderhart, D. L. *Science* **1984**, *223*, 283−285.
(2) Vanderhart, D. L.; Atalla, R. H. *Macromolecules* **1984**, *17*, 1465−1472.
(3) Sugiyama, J.; Vuong, R.; Chanzy, H. *Macromolecules* **1991**, *24*, 4168−4175.
(4) Atalla, R. H.; Hackney, J. M.; Uhlin, I.; Thompson, N. S. *Int. J. Biol. Macromol.* **1993**, *15*, 109−112.
(5) Hackney, J. M.; Atalla, R. H.; VanderHart, D. L. *Int. J. Biol. Macromol.* **1994**, *16*, 215−218.
(6) Yamamoto, H.; Horii, F.; Hirai, A. *Cellulose* **1996**, *3*, 229−242.
(7) Provasoli, L.; McLaughlin, J. J. A.; Droop, M. R. *Arch. Microbiol.* **1957**, *25*, 392−428.
(8) Belton, P. S.; Tanner, S. F.; Cartier, N.; Chanzy, H. *Macromolecules* **1989**, *22*, 1615−1617.
(9) Larrson, T.; Westermark, U.; Iverson, T. *Carbohydr. Res.* **1995**, *278*, 339−343.
(10) Yamamoto, H.; Horii, F.; Odani, H. *Macromolecules* **1989**, *22*, 4130−4132.
(11) Sugiyama, J.; Persson, J.; Chanzy, H. *Macromolecules* **1991**, *24*, 2461−2466.
(12) Yamamoto, H.; Horii, F. *Macromolecules* **1993**, *26*, 1313−1317.
(13) Throughout this study, the indexing refers to the unit cell proposed by Sugiyama et al.[3] The monoclinic indexing is represented by $(hkl)_m$, whereas the triclinic indexing is shown by $(hkl)_t$.
(14) Sugiyama, J.; Okano, T.; Yamamoto, H.; Horii, F. *Macromolecules* **1990**, *23*, 3196−3198.
(15) Mori, N.; Oikawa, T.; Katoh, T.; Miyahara, J.; Harada, Y. *Ultramicroscopy* **1988**, *25*, 195−202.
(16) Revol, J.-F. *Carbohydr. Polym.* **1982**, *2*, 123−134.
(17) Sugiyama, J.; Harada, H.; Fujiyoshi, Y.; Uyeda, N. *Planta* **1985**, *166*, 161−168.
(18) Sassi, J.-F.; Chanzy, H. *Cellulose* **1995**, *2*, 111−127.
(19) Sassi, J.-F. Ph.D. Thesis, Université Joseph Fourier Grenoble I, Grenoble, France, 1995; pp 57−73.
(20) Baker, A. A.; Helbert, W.; Sugiyama, J.; Miles, M. J. *J. Struct. Biol.* **1997**, *119*, 129−138.
(21) Hayashi, N.; Sugiyama, J.; Okano, T.; Ishihara, M. *Carbohydr. Res.* **1997**, *305*, 109−116.
(22) Kudlicka, K.; Brown, R. M., Jr.; Li, L.; Lee, J. H.; Kuga, S. *Plant Physiol.* **1995**, *107*, 111−123.
(23) Lee, J. H.; Brown, R. M., Jr.; Kuga, S.; Shoda, S.-I.; Kobayashi, S. *Proc. Natl. Acad. Sci. U.S.A.* **1994**, *91*, 7425−7429.
(24) Cousins, S. K.; Brown, R. M., Jr. *Polymer* **1995**, *36*, 3885−3888.

MA980664H